




Chrysophanol exhibits anti-cancer activities in lung cancer cell through regulating ROS/HIF-1 α /VEGF signaling pathway

Jie Zhang¹ · Qian Wang^{1,2} · Qiang Wang¹ · Peng Guo¹ · Yong Wang¹ · Yuqing Xing¹ · Mengmeng Zhang¹ · Fujun Liu¹ · Qingyun Zeng² 

Received: 28 July 2019 / Accepted: 27 September 2019
© Springer-Verlag GmbH Germany, part of Springer Nature 2019

Abstract

In the present study, we explored the anti-tumor and anti-angiogenesis effects of chrysophanol, and to investigate the underlying mechanism of the chrysophanol on anti-tumor and anti-angiogenesis in human lung cancer. The viability of cells was measured by CCK-8 assay, cell apoptosis was measured by Annexin-FITC/PI staining assay, and the cell migration and invasion were analyzed by wound-healing assay and transwell assay. ROS generation and mitochondrial membrane potential were analyzed by DCFH-DA probe and mitochondrial staining kit. Angiogenesis was analyzed by tube formation assay. The expression of CD31 was analyzed by immunofluorescence. The levels of proteins were measured by western blot assay. The anti-tumor effects of chrysophanol in vivo were detected by established xenograft mice model. In this study, we found that the cell proliferation, migration, invasion, tube formation, the mitochondrial membrane potential, and the expression of CD31 were inhibited by chrysophanol in a dose-dependent manner, but cell apoptotic ratios and ROS levels were increased by chrysophanol in a dose-dependent manner. Furthermore, the effects of chrysophanol on A549, H738, and HUVEC cell apoptotic rates were reversed by the ROS inhibitor NAC. Besides, the effects of chrysophanol on HUVEC cell tube formation were reversed by the HIF-1 α inhibitor KC7F2 and the VEGF inhibitor axitinib in vitro. Moreover, tumor growth was reduced by chrysophanol, and the expression of CD31, CD34, and angiogenin was suppressed by chrysophanol in vivo. Our finding demonstrated that chrysophanol is a highly effective and low-toxic drug for inhibition of tumor growth especially in high vascularized lung cancer.

Keywords Angiogenesis · Invasion · Metastasis · Tube formation

Introduction

Lung cancer is the second malignant cancer in the world, and characterized as high fatality rate, and diagnosed in advanced stages (Liam et al. 2015). It also has a higher incidence rate in both men and women (Huang et al. 2015). In present, surgery, radiotherapy, and chemotherapy are the common methods for lung cancer treatment (Naylor et al. 2016; Hirsch et al. 2017). But it usually causes poor prognosis and chemo-resistance or

multidrug-resistant after treatment by surgery, radiotherapy, and chemotherapy (Kim 2016; Keba et al. 2018). Therefore, it is essential to explore new treatment strategies for lung cancer.

Angiogenesis is one of the hallmarks of solid cancer (Ramjiawan et al. 2017). Angiogenesis as the foundation of the tumor cell proliferation, migration, and invasion in the cancer progression (Viallard and Larrivee 2017), and it also continually provides nutrients and oxygen to cancer cell growth (Njah et al. 2019). Hypoxia is the main characteristic of the tumor microenvironment (TME); hypoxia also is the trigger of the angiogenesis which increases hypoxia-induced factors (HIFs) to recruit the multiple pro-angiogenic factors (Irwin et al. 2009, Li et al., 2019). Therefore, anti-angiogenesis may be an efficient approach to anti-tumor.

In recent years, traditional Chinese medicine and effective components have been shown high efficacy, low toxicity, and low adverse effects in tumor treatment. Chrysophanol belongs to the anthraquinone family, and a natural active ingredient

✉ Qingyun Zeng
qingyunzengjnsd@163.com

Qian Wang
qingyunzengjnsd@163.com

¹ Shandong Provincial Hospital affiliated to Shandong University, Jinan 250021, Shandong, China

² Hospital Affiliated to Shandong University of Traditional Chinese Medicine, Jinan 250011, Shandong, China

from *Rheum palmatum* L., *Rumex dentatus*, and *Polygonum cuspidatum* (Song et al. 2019). It has been reported that the anthraquinone family, including aloe-emodin, emodin, rhein, chrysophanol, and physcion, shows the anti-tumor effects in multiple tumor types through regulating cell proliferation, apoptosis, migration, and invasion (Lim et al. 2017; Lim et al. 2018). The previous study indicates that chrysophanol suppresses choriocarcinoma through inducing apoptosis via regulating ROS, AKT, and ERK1/2 pathways (Lim et al. 2017). And chrysophanol inhibits ovarian cancer through overloading mitochondrial calcium to inducing cell death and inhibit cell invasion (Lim et al. 2018). Moreover, chrysophanol inhibits breast cancer by inhibiting proliferation and inducing apoptosis via NF- κ B/cyclin D and NF- κ B/Bcl-2 signaling cascade (Ren et al. 2018). Provoking, emodin inhibits anaplastic thyroid cancer, human pancreatic cancer, and colonic cancer by suppressing angiogenesis (Braumann et al. 2017; Hu et al. 2017; Shi and Zhou 2018). Besides, aloe-emodin and rhein also have been reported to inhibit multiple tumors by suppressing angiogenesis (Fernand et al. 2011; He et al. 2011; Wu et al. 2016; Chen et al. 2018). However, it was unknown if chrysophanol inhibits tumors by inhibiting angiogenesis.

In the present study, we explored the anti-tumor and anti-angiogenesis effects of chrysophanol and revealed the underlying mechanism of chrysophanol anti-tumor and anti-angiogenesis.

Material and methods

Chemical and reagents

Chrysophanol (chrysophanic acid), the ROS inhibitor N-acetyl-L-cysteine (NAC), the HIF-1 α inhibitor KC7F2, the VEGF inhibitor axitinib, and cisplatin (DDP) were purchased from Selleck (Houston, TX, USA). Cell Counting Kit-8 and DMSO were purchased from Sigma-Aldrich (Louis, MO, USA). Matrigel and FITC Annexin V Apoptosis Detection kit were purchased from Becton Dickinson (BD, NJ, USA). RPMI 1640 medium and fetal bovine serum (FBS) were purchased from Thermo Fisher Scientific (MA, USA). JC-1 kit and reaction oxygen species (ROS) assay kit were purchased from Beyotime Biotechnology (Shanghai, China). Antibodies were purchased from Cell Signaling Technology (MA, USA) and Abcam (Cambridge, UK).

Cell lines and culture

The human lung cancer cell lines A549 and H738 and the human vascular endothelial cell line HUVEC were purchased from the American Type Culture Collection (ATCC, MD, USA). The cells were maintained in RPMI 1640 medium

suspended with 10% FBS, 10 μ g/mL streptomycin, and 10 U/mL penicillin. All cells were cultured in an incubator with 5% CO₂ at 37 °C.

CCK-8 assay

The cell viability was measured using the CCK-8 kit following the manufacturer's protocols. In brief, A549 and H738 cells were plated on 24-well plates at a density of 1×10^5 cells/well. Chrysophanol was dissolved in DMSO, and then cells were treated with 0, 1, 2, 5, 10 μ M chrysophanol for 24 h and 48 h. Then CCK-8 solution was added into each well and the absorbance of each well was detected at 450 nm using a microplate reader.

Apoptosis assay

Apoptosis of A549 and H738 cells induced by chrysophanol was measured by flow cytometry using a FITC Annexin V Apoptosis Detection kit (BD, NJ, USA) according to the manufacturer's instrument. Briefly, A549 and H738 cells were plated on 24-well plates at a density of 1×10^5 cells/well and treated with 2 μ M and 4 μ M for 24 h and 48 h. Then cells were harvested and incubated in 400 μ L binding buffer with 5 μ L FITC and 5 μ L propidium iodide (PI) in the dark for 15 min at temperature (18–26 °C). Next, the stained cells were analyzed using a flow cytometer (BD, NJ, USA).

Western blotting

Cells were harvested and lysed with RIPA buffer containing protease inhibitor (Thermo Fisher Scientific, MA, USA). The concentration of protein was measured using a BCA Protein Assay kit (Beyotime, Shanghai, China). Then 3 μ g protein lysates were separated using SDS-PAGE and transferred to PVDF membranes. The membranes were blocked for 1 h at room temperature (18–26 °C) with blocking buffer (5% milk, 0.5% Tween20, 1 \times Tris-buffered saline). The members followed by washed with wash buffer (0.5% Tween20, 1 \times Tris-buffered saline) and incubated with special primary antibodies (Ki67, 1:2000, Abcam, ab16667; PCNA, 1:1000, Cell Signaling Technology, 13110; Bax, 1:1000, Cell Signaling Technology, 2772; Bcl-2, 1:2000, Abcam, ab182858; cleaved-caspase3, 1:1000, Cell Signaling Technology, 9664; cleaved-caspase9, 1:100, Abcam, ab2324; cleaved-PARP, 1:2000, Abcam, ab32046; MMP-2, 1:1000, Cell Signaling Technology, 87809; MMP-9, 1:1000, Cell Signaling Technology, 13667; TIMP-3, 1:1000, Cell Signaling Technology, 5673; E-cadherin, 1:1000, Cell Signaling Technology, 3195; N-cadherin, 1:1000, Cell Signaling Technology, 13116; Vimentin, 1:1000, Cell Signaling Technology, 5741; HIF-1 α , 1:1000, Cell Signaling Technology, 14179; VEGF, 1:1000, Cell Signaling

Technology, 9698; Vasohibin-1, 1:1000, Abcam, ab199732; GAPDH, 1:1000, Cell Signaling Technology, 4970) overnight at 4 °C. Then the membranes were washed with wash buffer and probed with special secondary antibody HRP-labeled Goat Anti-Rabbit IgG (H+L) (1:1000, Beyotime, A0208) for 1 h at room temperature (18–26 °C), and visualized by ECL kit (BioRad, CA, USA). Bands were quantified by the Image Analysis software (BioRad, CA, USA).

Wound-healing assay

A549, H738, and HUVEC cells were plated on 24-well plates at a density of 1×10^5 cells/well overnight, and then cells were treated with 2 μ M and 4 μ M chrysophanol for 48 h. Then the cells were harvested and plated on 6-well plates at a density of 1×10^5 cells/well, the scratch wound was marked using 200- μ L pipette tip, and the floating cells were washed away with PBS. The scratch was observed and imaged using an inverted microscope (Olympus, Tokyo, Japan) at 0 h and 48 h. The healing wound area was quantified using Image J software (Version X; Media Cybernetics, Silver Springs, MD, USA).

Transwell assay

The transwell inserts (8- μ m pore; Corning, MA, USA) were used for invasion assay. The upper chambers were coated with 0.1% Matrigel (BD, NJ, USA) for 30 min at 37 °C. Meanwhile, A549, H738, and HUVEC cells were harvested and resuspended with serum-free RPMI 1640 medium containing 0.1% BSA and plated on the upper chambers at a density of 1×10^5 cells/well, and then cells were treated with 2 μ M and 4 μ M chrysophanol for 48 h. After 48 h, the noninvaded cells located at the front surface of the filter were removed using a cotton swab, and the invaded cells at the opposite surface of the filter were stained with 0.1% crystal violet for 20 min. The invaded cells were imaged using an inverted microscope (Olympus, Tokyo, Japan), and quantified in five random fields per well.

Tube formation assay

Tube formation assay was carried out with reference to the previous studies (Li et al. 2019a, b). In brief, HUVEC were harvested and resuspended with PBS at a density of 1×10^5 cells/well and treated with 2 μ M and 4 μ M chrysophanol for 30 min. Cells were then plated on the 24-well plates pre-coated with Matrigel (BD, NJ, USA) and incubated for 8 h at 37 °C. Then the tubular structures were observed and imaged using an inverted microscope (Olympus, Tokyo, Japan), and the tuber formation was quantified by counting the number of the tube.

Immunofluorescence

HUVEC cells were harvested and pretreated with 2 μ M and 4 μ M chrysophanol for 30 min before plated on 24-well plates at a density of 1×10^5 cells/well overnight. Cells were then harvested and fixed with 4% paraformaldehyde (PFA) for 20 min, then permeabilized with PBS containing 0.2% Triton X-100 for 10 min and blocked with PBS containing 2% bovine serum albumin (BSA, Solarbio, Beijing, China) for 1 h at room temperature (18–26 °C). Following, cells were incubated with special primary antibodies: anti-CD31 antibody (1:500, Abcam, ab28364), anti-CD34 antibody (1:300, Abcam, ab81289), anti-angiogenin antibody (1:500, Abcam, ab10600) for 24 h at 4 °C. After 24 h, the cells were washed with PBS and incubated with special secondary antibody (goat anti-rabbit IgG H&L, Invitrogen, CA, USA) for 1 h at room temperature (18–26 °C). Finally, cells were washed with PBS containing 0.1% BSA and stained with 4',6-diamidino-2-phenylindole (DAPI) for 10 min at room temperature (18–26 °C), and cells were observed and imaged using a confocal fluorescence microscope (UltraView Vox; PerkinElmer, MA, USA).

ROS detection

The 2',7'-dichlorofluorescein diacetate (DCFH-DA) was used for ROS detection in this study as described previous study (Kitajima et al. 2016). Briefly, A549, H738, and HUVEC cells were treated with 2 μ M and 4 μ M chrysophanol and then cells were stained with 20 μ M DCFH-DA for 30 min in the dark. The fluorescence intensity of DCF was detected by flow cytometry.

Mitochondrial membrane potential analysis

Mitochondrial membrane potential ($\Delta\Psi$ m) was measured using the mitochondrial staining kit (Sigma-Aldrich, MO, USA) as the previous study according to the manufacturer's protocol (Koyuncu et al. 2018). Briefly, A549, H738, and HUVEC cells were plated on 24-well plates at a density of 1×10^5 cells/well and treated with 2 μ M and 4 μ M chrysophanol for 24 h at 37 °C. After 24 h, the cells were harvested and stained with staining buffer with JC-1 for 20 min at 37 °C. The cells were then harvested and resuspended in 1 mL staining buffer. Both red and green fluorescence intensity was detected by flow cytometry.

Immunohistochemical

The immunohistochemical (IHC) was performed as previously described (Hsiao et al. 2019). In brief, the tumor slices were blocked by PBS containing 5% BSA and 0.3% Triton X-100 for 30 min at 37 °C. The slices were incubated with primary antibodies: anti-CD31 antibody (1:500, Abcam, ab28364), anti-CD34 antibody (1:300, Abcam, ab81289), and anti-

angiogenin antibody (1:500, Abcam, ab10600) for 24 h at 4 °C. After 24 h, the slices then were washed with PBS containing 0.1% Tween 20 and incubated with secondary antibody (goat anti-rabbit IgG H&L, Invitrogen, CA, USA) for 30 min at room temperature (18–26 °C). The slides were observed and imaged using a confocal fluorescence microscope (UltraView Vox; PerkinElmer, MA, USA).

Animal experiment

All animal experiments of this study were proved by the Animal Care Ethics Committee of Shandong Provincial Hospital affiliated to Shandong University (No.

2018050124). The four to 6-week-old male C57BL/6 nude mice were randomly divided into four groups: control group (equal volumes of saline), 10-mg/kg chrysophanol group, 20-mg/kg chrysophanol group, 0.2-mg/kg cisplatin group. A549 cells were subcutaneously injected into the flank of nude mice; the number of mice each group was six. There was oral administration of chrysophanol, and tail vein injection of cisplatin every other day for 4 weeks. We weighed the mice every week until mice were sacrificed. After 4 weeks, mice were sacrificed, and the tumors were separated, then the tumor weight was measured by electronic balance, and volume was quantified using a vernier caliper. The part of the tumor was stored for IHC analysis.

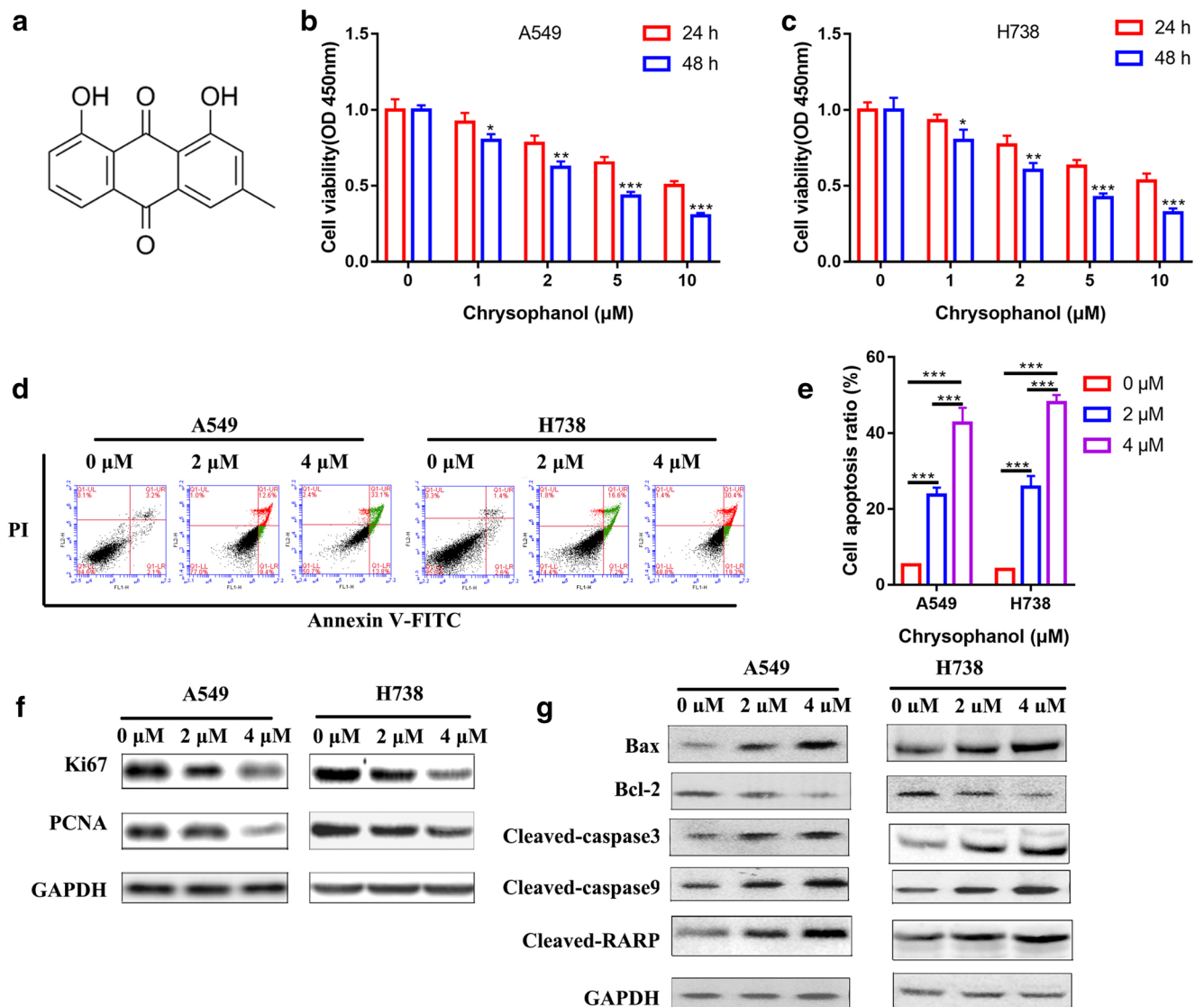


Fig. 1 Chrysophanol suppresses lung cancer cell proliferation and induces apoptosis in vitro. **a** The chemical structure of chrysophanol. **b**, **c** The A549 and H738 cell proliferation after treatment with different concentration of chrysophanol (0, 1, 2, 5, 10 μM) were measured by CCK-8 assay at 24 h and 48 h. **d**, **e** The apoptotic ratios after treatment with 2 μM and 4 μM for 48 h were detected using Annexin V-FITC/PI

staining by flow cytometry. **f**, **g** A549 and H738 were treatment with 2 μM and 4 μM for 48 h; the levels of proliferation-related proteins (Ki67 and PCNA) and levels of apoptosis-related proteins (Bax, Bcl-2, cleaved-caspase3, cleaved-caspase9, and cleaved-PARP) were determined by western blotting. Data were presented as mean ± SD. * $P < 0.05$, ** $P < 0.01$, *** $P < 0.001$

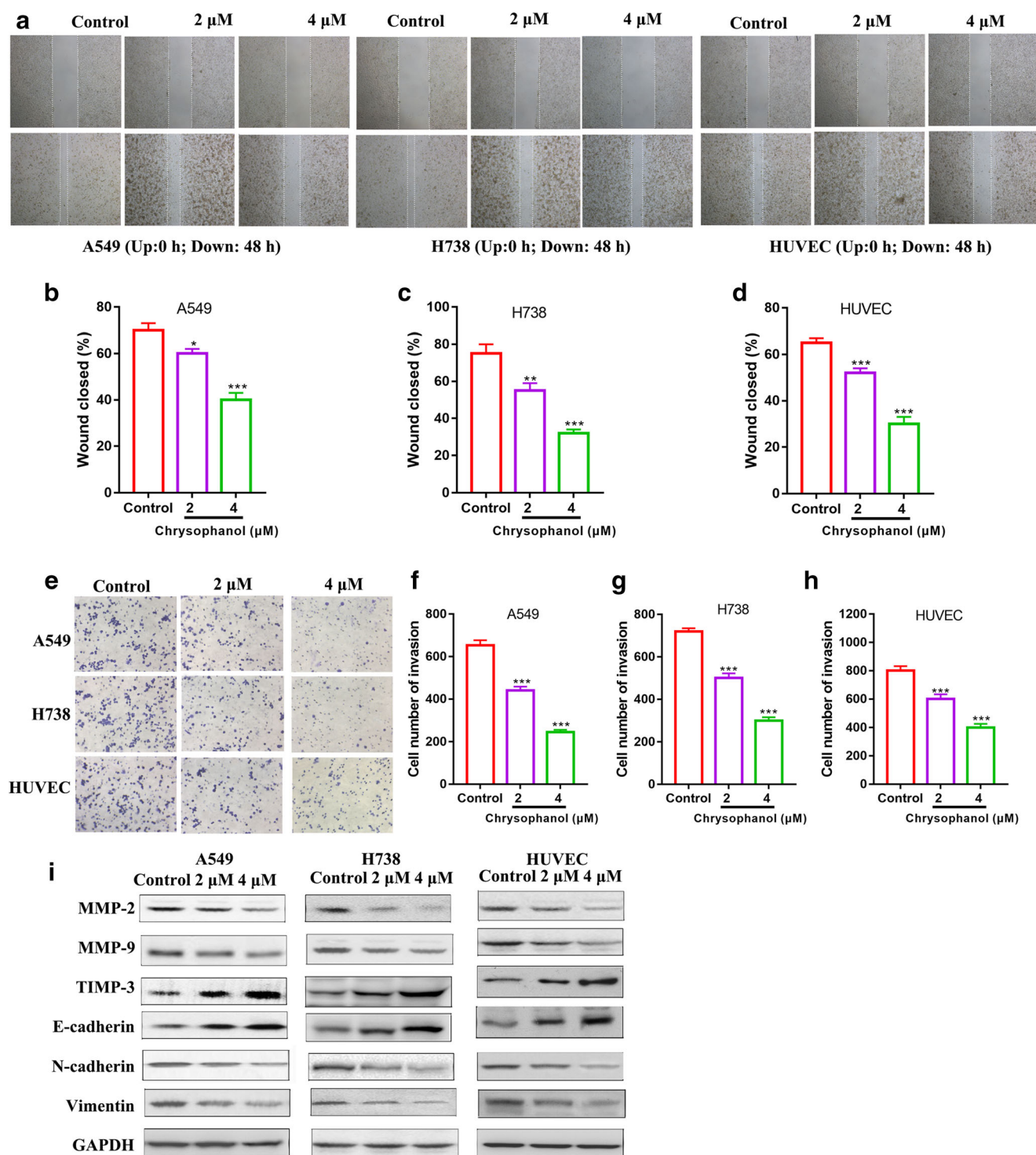


Fig. 2 Chrysophanol suppresses lung cancer cells and endothelial cell migration and invasion in vitro. A549, H738, and HUVEC were treated with 2 μ M and 4 μ M for 48 h. **a–d** The cell migration was analyzed by wound-healing assay. **e–h** The cell invasion was measured

by transwell assay. **i** The protein levels of MMP-2, MMP-9, TIMP-3, E-cadherin, N-cadherin, and vimentin were determined by western blotting. Data were presented as mean \pm SD. * P < 0.05, ** P < 0.01, *** P < 0.001

Statistical analysis

SPSS 20.0 and GraphPad Prism 7.0 were used for statistical analysis. The data were presented as mean \pm SD.

The Student's t test and one-way analysis of variance (ANOVA) were used for comparison of differences of two or more groups. P < 0.05 was considered the statistical significance.

Results

Chrysophanol suppresses lung cancer cell proliferation and induces apoptosis in vitro

The chemical structure of chrysophanol is shown in Fig. 1 a. The viability of A549 and H738 cells was gradually suppressed by increasing chrysophanol concentration (Fig. 1b, c). The IC₅₀ value of chrysophanol treatment of A549 at 48 h was 3.50 μ M, and the IC₅₀ value of chrysophanol treatment of H738 at 48 h was 4.00 μ M. Thus, the concentrations of 2 μ M and 4 μ M were chosen for subsequent experiments. The apoptotic ratios of A549 and H738 cells were significantly increased by the growing concentration of chrysophanol (Fig. 1d, e). The results of western blotting also showed that cell proliferation-related proteins Ki-67 and PCNA were remarkably decreased by increasing contraction of

chrysophanol (Fig. 1f). Similarly, the proapoptotic proteins Bax, caspase 3, caspase 9, and PARP were significantly activated, and the anti-apoptotic protein Bcl-2 was inhibited by chrysophanol (Fig. 1g). Our finding indicates that the chrysophanol inhibits lung cancer cell proliferation and induces lung cancer cell apoptosis in a dose-dependent way.

Chrysophanol suppresses lung cancer cells and endothelial cells migration and invasion in vitro

To further investigate the effects of chrysophanol on the migration and invasion of A549, H738, and HUVEC cells, we found that the cell migration and invasion both lung cancer cells and endothelial cells were suppressed by chrysophanol in a dose-dependent manner (Fig. 2a–h). Furthermore, the protein levels of MMP-2, MMP-9, N-cadherin, and vimentin were significantly decreased, and the protein levels of TIMP and E-cadherin

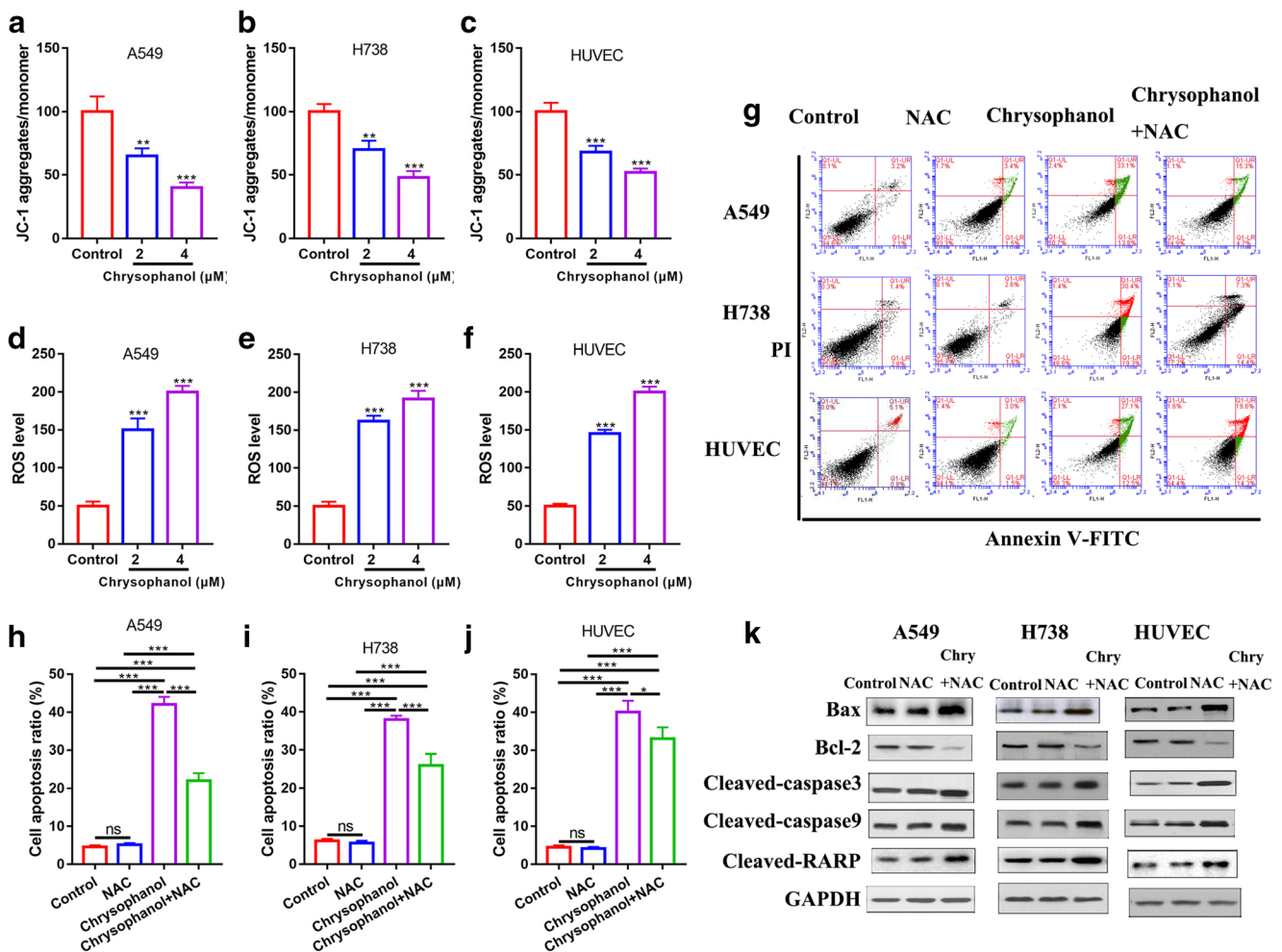


Fig. 3 Chrysophanol induces cell apoptosis by ROS accumulation in vitro. A549, H738, and HUVEC were treatment with 2 μ M and 4 μ M for 48 h. **a–c** The mitochondrial membrane potential of the cells was measured by mitochondrial staining kit. **d–f** The ROS generation was detected by DCFH-DA probe. A549, H738, and HUVEC were treatment with 2 μ M and 4 μ M chrysophanol, and treatment with 5 μ M NAC for 48

h. **g–j** The cell apoptosis was detected using Annexin V-FITC/PI staining by flow cytometry. **k** The levels of apoptosis-related proteins (Bax, Bcl-2, cleaved-caspase3, cleaved-caspase9, and cleaved-PARP) were determined by western blotting. Data were presented as mean \pm SD. * P < 0.05, ** P < 0.01, *** P < 0.001

were strongly increased by chrysophanol in a dose-dependent manner (Fig. 2i). These results suggested that the migration and invasion of lung cancer cells and endothelial cells were significantly inhibited by chrysophanol in a dose-dependent manner.

Chrysophanol induces cell apoptosis by ROS accumulation in vitro

To further investigate the induction of cell apoptosis mechanism of chrysophanol, the mitochondrial membrane potential of A549, H738, and HUVEC cells was detected using the JC-1 by flow cytometry. Results showed that the mitochondrial membrane potential of A549, H738, and HUVEC cells was gradually decreased by chrysophanol in a dose-dependent way (Fig. 3a–c). Also, the ROS levels of A549, H738, and HUVEC cells were significantly increased by chrysophanol in a dose-dependent way (Fig. 3d–f). Moreover, the apoptotic ratios of A549, H738, and HUVEC cells were decreased by ROS inhibitor NAC but increased by chrysophanol, and the proapoptotic effects of chrysophanol were reversed by NAC (Fig. 3g–j). Consistently, the proapoptotic proteins Bax, caspase 3, caspase 9, and PARP were significantly activated by chrysophanol and inhibited by NAC, and the anti-apoptotic protein Bcl-2 was inhibited by chrysophanol and promoted by NAC, and the effects of chrysophanol on protein levels were reversed by NAC (Fig. 3k). Our results indicate that chrysophanol promoted ROS accumulation in the mitochondrial membrane to decrease the mitochondrial membrane potential lead to cell apoptosis.

Chrysophanol suppresses tube formation in vitro

Previous experiments showed chrysophanol inhibited HUVEC cell migration and invasion and induced cell apoptosis by

accumulating ROS. Then we continued to investigate the effects of chrysophanol on angiogenesis in vitro. Our finding showed that vascular networks of HUVEC were disrupted by chrysophanol in a dose-dependent way (Fig. 4a, b). Besides, the immunofluorescence intensity of CD31 was significantly suppressed by chrysophanol in a dose-dependent way (Fig. 4c, d). And the protein levels of HIF-1 α and VEGF were significantly inhibited, and the protein level of vasohibin was increased by chrysophanol in a dose-dependent manner (Fig. 4e). Our finding suggested that chrysophanol inhibited angiogenesis in vitro in a dose-dependent manner.

Chrysophanol inhibits endothelial cell angiogenesis through HIF-1 α /VEGF signaling pathway in vitro

To further investigate the mechanism of chrysophanol inhibition of endothelial cell angiogenesis, our finding showed that chrysophanol, the HIF-1 α inhibitor KC7F2, and VEGF inhibitor axitinib significantly inhibited tube formation; furthermore, chrysophanol enhanced the inhibition effects of the KC7F2 and axitinib on tube formation (Fig. 5a, b). Moreover, the immunofluorescence intensity of CD31 was significantly inhibited by chrysophanol, KC7F2, and axitinib, and chrysophanol enhanced the inhibition effects of KC7F2 and axitinib on immunofluorescence intensity of CD31 (Fig. 5c, d). Moreover, the accumulation of the ROS was increased by chrysophanol, KC7F2, and axitinib, and the chrysophanol enhanced the effects of KC7F2 and axitinib on ROS accumulating (Fig. 5e). The protein levels of HIF-1 α and VEGF were significantly inhibited, and the protein level of vasohibin was increased by chrysophanol, KC7F2, and axitinib; the effects of KC7F2 and axitinib were enhanced by chrysophanol (Fig. 4e). These results

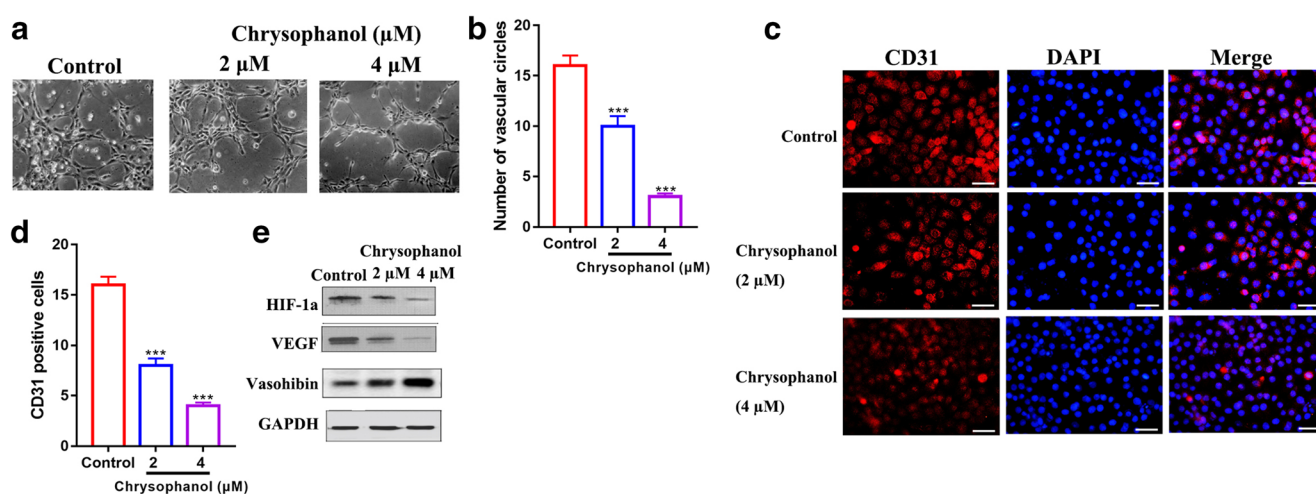


Fig. 4 Chrysophanol suppresses tube formation in vitro. HUVEC was treatment with 2 μ M and 4 μ M chrysophanol for 48 h. **a**, **b** Tube formation was used to measure the capacity of the angiogenesis. **c**, **d** The cell immunofluorescence was used to detect the expression of

CD31. **e** Western blot was used to determine the protein levels of HIF-1 α , VEGF, and vasohibin. Data were presented as mean \pm SD. * P < 0.05, ** P < 0.01, *** P < 0.001

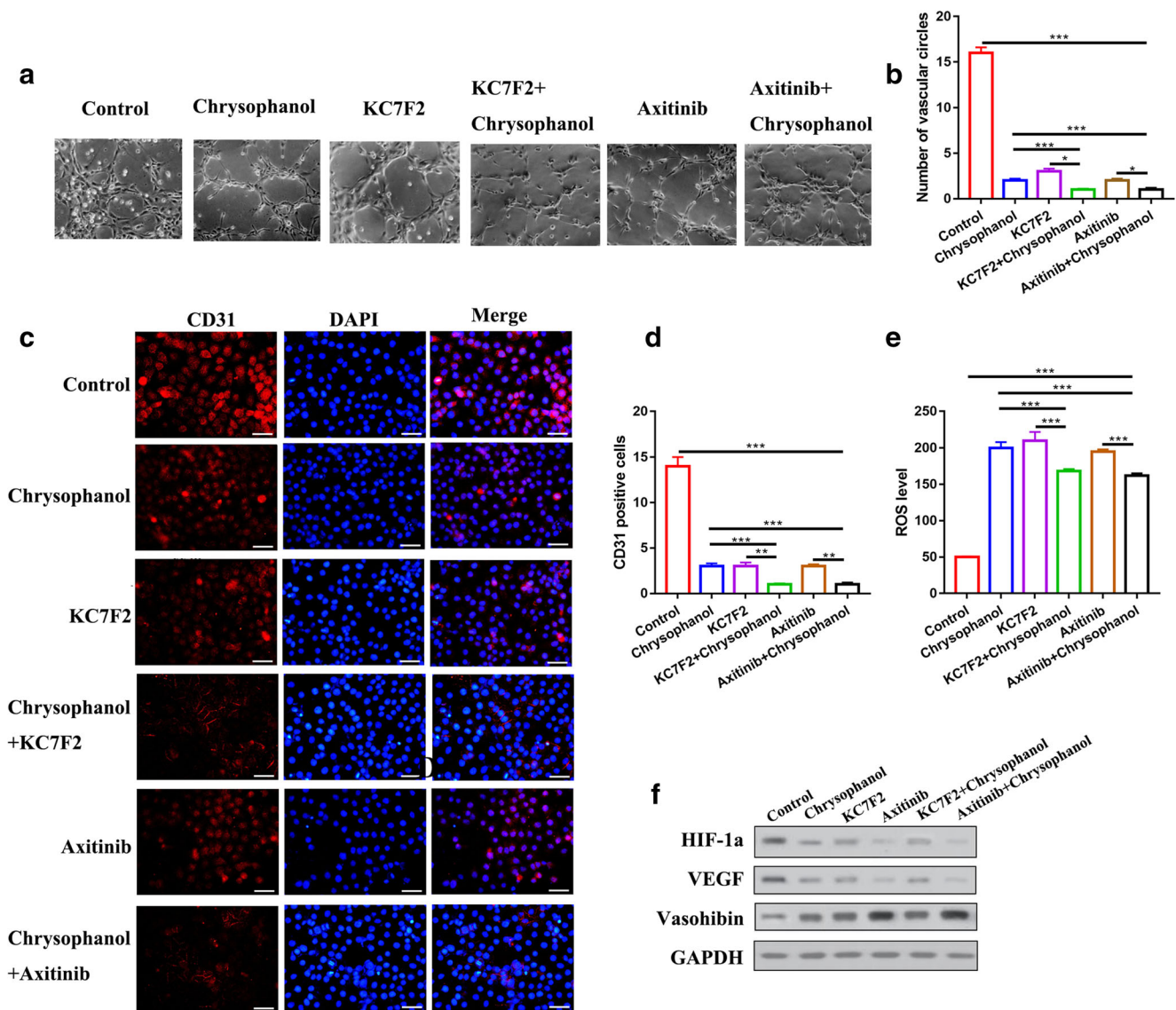


Fig. 5 Chrysophanol inhibits endothelial cell angiogenesis through HIF-1 α /VEGF signaling pathway in vitro. HUVEC was treatment with 4 μ M chrysophanol, 10 μ M KC7F2, and 0.1 nM axitinib for 48 h. **a, b** Tube formation was used to measure the capacity of the angiogenesis. **c, d** The cell immunofluorescence was used to detect the expression of CD31. **e**

suggested that chrysophanol inhibited endothelial cell angiogenesis through HIF-1 α /VEGF signaling pathway in vitro.

Chrysophanol inhibits tumor growth and angiogenesis in vivo

To explore the anti-tumor and anti-angiogenic effects of the chrysophanol in vivo, the xenograft mice model was employed in our study. Tumor weight and volume were significantly decreased by DDP, and by chrysophanol in a dose-dependent manner (Fig. 6a–d). However, DDP inhibited tumor growth and also significantly reduced the body weight of the mice; on the contrary, chrysophanol anti-tumor growth

The ROS generation was detected by DCFH-DA probe. **f** The protein levels of HIF-1 α VEGF and vasohibin were measured by western blotting. Data were presented as mean \pm SD. * P < 0.05, ** P < 0.01, *** P < 0.001

showed a milder manner (Fig. 6b). Besides, we found that chrysophanol significantly suppressed the expression of CD31, CD34, and angiogenin in tumor tissues (Fig. 6e–h). Our results indicated that chrysophanol showed the effects of anti-tumor and anti-angiogenic in vivo, and chrysophanol was a high efficacy and low-toxicity anti-tumor molecule.

Discussion

Lung cancer is the leading cause of cancer death in both men and women in the world (Torre et al. 2016). It is characteristic with high aggressive results in late accurate diagnosis and

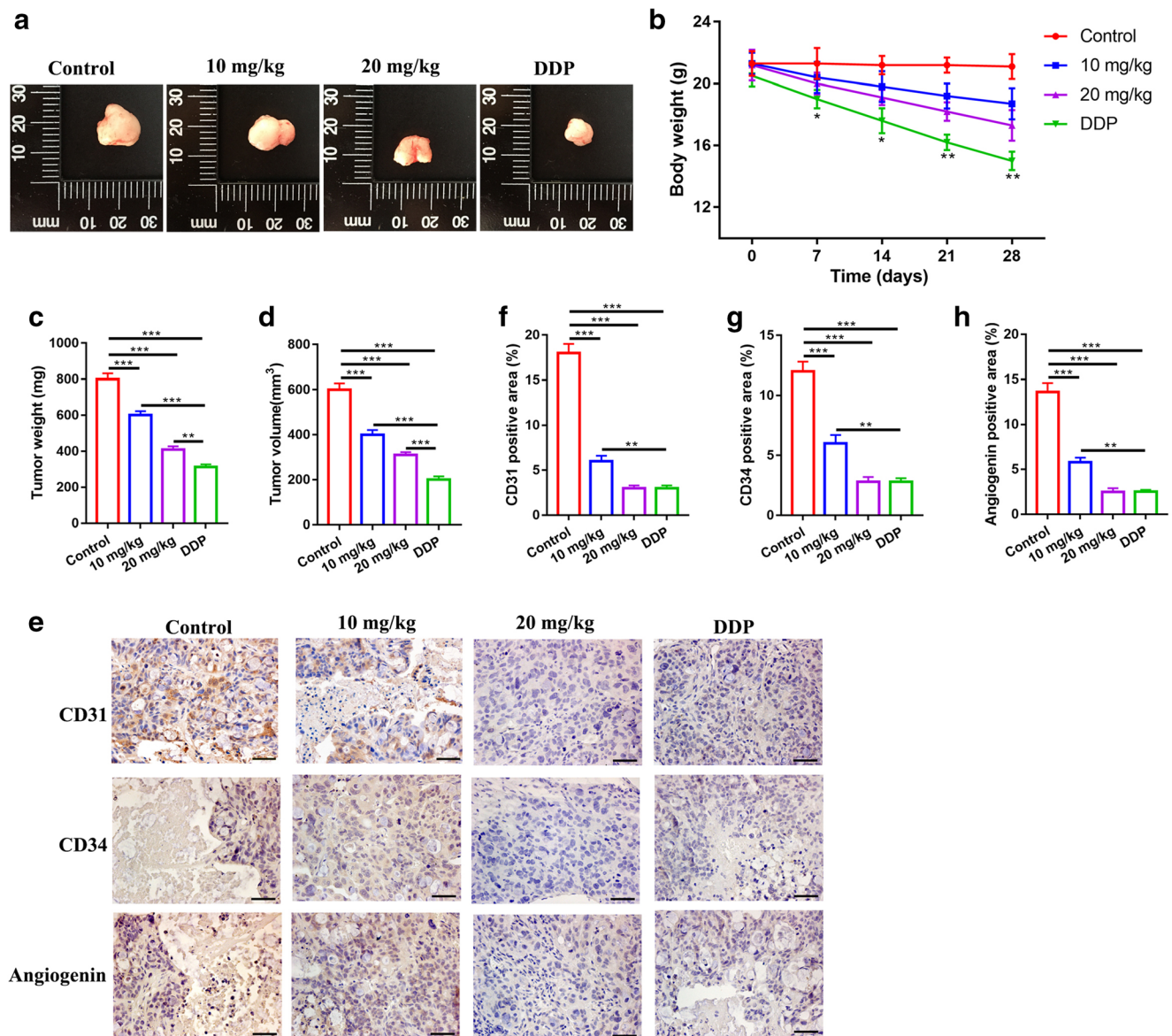


Fig. 6 Chrysophanol inhibits tumor growth and angiogenesis in vivo. A549 cells were subcutaneously injected into the flank of nude mice, oral administration of 10 mg/kg chrysophanol, 20 mg/kg chrysophanol, and tail vein injection of 0.2 mg/kg cisplatin ($n = 6$) every other day for 4 weeks. **a** The tumors were isolated from mice. **b** The body weight of mice

was detected by electronic balance. **c, d** Tumor volume was measured by vernier caliper. **e–h** The expression of CD31, CD34, and angiogenic was analyzed by immunohistochemistry. Data were presented as mean \pm SD. * $P < 0.05$, ** $P < 0.01$, *** $P < 0.001$

poor prognosis (Frezzetti et al. 2017). In China, environmental pollution, food, genetics, chronic obstructive pulmonary, smoking, and exposure to secondhand smoking are the primary cause leading to lung cancer (Hong et al. 2015; Chen et al. 2017; Zou et al. 2017). Despite increasing the treatments of lung cancer, the incidence and mortality of lung cancer remain increased (Torre et al. 2016). In the present study, results revealed the anti-tumor effects of chrysophanol on lung cancer cell in vitro and in vivo. We also exposed the anti-angiogenesis function of the chrysophanol on HUVEC in lung cancer. Moreover, we demonstrated that chrysophanol inhibited proliferation, migration, and invasion, and induced

apoptosis of lung cancer cells. Also, we demonstrated chrysophanol suppressed angiogenesis in lung cancer. And we confirmed that chrysophanol increased ROS accumulation and loss of the mitochondrial membrane potential to induce apoptosis and angiogenesis. We further revealed the mechanism of anti-tumor and anti-angiogenesis effects of chrysophanol in lung cancer (Fig. 7).

In the present study, chrysophanol suppressed lung cancer cell A549 and H738 proliferation in a time- and dose-dependent manner, and significantly reduced the protein levels of the Ki67 and PCNA; the results are consistent with previous studies (Lee et al. 2011; Ren et al. 2018). The

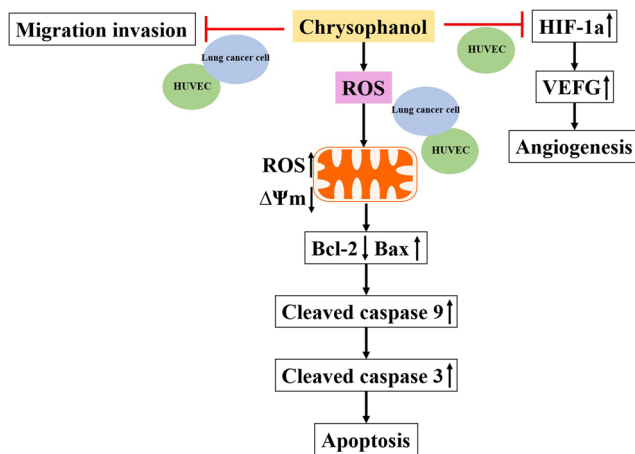


Fig. 7 The schematic diagram of the anti-tumor and anti-angiogenesis function of chrysophanol by targeting multiple signaling pathways

viability of the tumor cell proliferative activity is the most important marker in tumor progression; Ki67 and PCNA are commonly used to assess the cell growth fraction (Jurikova et al. 2016). Our results suggested that chrysophanol anti-tumor inhibits cell proliferation. Chrysophanol induces cell apoptosis which has been reported in multiple human malignancies. In breast cancer cells, chrysophanol anti-tumor by inhibiting proliferation induces apoptosis through NF- κ B/cyclin D1 and NF- κ B/Bcl-2 signaling cascade (Ren et al. 2018). It has been reported that chrysophanol induces choriocarcinoma cell apoptosis by inducing ROS media in the mitochondrial apoptosis pathway (Lim et al. 2017). In our study, we found that chrysophanol induced apoptosis in a time- and dose-dependent manner; the proapoptotic protein Bax, cleaved-caspase 3, cleaved-caspase 9, and cleaved-RARP were significantly increased, and the anti-apoptotic protein Bcl-2 was reduced by chrysophanol. We also found that chrysophanol increased ROS generation and repressed the mitochondrial membrane potential in both the lung cancer cell and HUVEC. Our results suggested that chrysophanol induced lung cancer cell apoptosis by triggering mitochondria apoptosis pathway.

Tumor progression involves migration, invasion, adhesion, proliferation, and angiogenesis (Cheng et al. 2014; Liu et al. 2017). Also, tumor progression triggers epithelial-mesenchymal transformation (EMT), cell reprogramming, and progressive changes in metabolism (Biswas 2015; Izgi et al. 2017; Netea-Maier et al. 2018). In this study, we demonstrated that the migration and invasion of A549, H738, and HUVEC were markedly decreased by chrysophanol in a dose-dependent way. Moreover, chrysophanol significantly inhibited the protein levels of MMP-2 and MMP-9 and increased the protein levels of TIMP-3 of A549, H738, and HUVEC in a dose-dependent manner. MMP-2 and MMP-9 belong to extracellular proteolytic proteases which play an important role in tumor invasion (Shay et al. 2015; Merchant et al. 2017). Besides, the protein levels of

the epithelial marker E-cadherin of A549, H738, and HUVEC were upregulated, and the protein levels of the mesenchymal markers N-cadherin and vimentin of A549, H738, and HUVEC were reduced by chrysophanol in a dose-dependent manner. Our finding suggested that chrysophanol anti-tumor and anti-angiogenesis blocked the migration and invasion progression in lung cancer.

Angiogenesis is a key fundamental progression in the tumor growth; it plays an important role in triggering dormant tumor transits to malignant tumor state, and a potential pathway to promoting tumor cell migration and invasion (Kang et al. 2018). And the migration of the HUVEC is an early step for the sprouting and elongation of a newly formed vessel. Thus, angiogenesis may be a crucial potential target for treatment. It has been reported that it is efficient if anti-angiogenic therapy combines with immune therapy to anti-tumor in renal cancer (Kuusk et al. 2017). It also reports angiogenesis promoting non-small-cell lung cancer (NSCLC) growth (Mao et al. 2015; Mao et al. 2019). In breast cancer, FOXM1 interact with HMGA1 in promoting tumor angiogenesis to support breast cancer aggressiveness (Zanin et al. 2019). And in ovarian cancer, inhibiting the angiogenesis-related microRNA can suppress tumor growth (Chen et al. 2019). In this study, chrysophanol suppressed the invasion capacity of the lung cancer cell and HUVEC, the activity of MMPs, and the capacity of the tube formation in vitro in a dose-dependent manner. And more, chrysophanol reduced the CD31, HIF-1 α , and VEGF expression levels, and increased the vasohibin expression level in a dose-dependent manner. Moreover, we demonstrated that the angiogenesis was reduced not only by HIF-1 α inhibitor KC7F2 and VEGF inhibitor axitinib but also by chrysophanol. Importantly, chrysophanol enhanced the inhibition effects of the KC7F2 and axitinib to anti-angiogenesis. These results suggested that chrysophanol anti-angiogenesis in lung cancer regulates HIF-1 α /VEGF signaling pathway.

Conclusion

In summary, our study showed that chrysophanol anti-tumor represses cell proliferation, migration, invasion, and angiogenesis in lung cancer by regulating every stage of tumor progression-related proteins and pathway. It is suggested that chrysophanol is an efficient treatment agent for lung cancer treatment, particularly in high vascularized tumors.

Author contribution Jie Zhang and Qian Wang performed the experiences.

Qiang Wang, Peng Guo, and Yong Wang performed some experiences and analyzed the data.

Yuqing Xing, Mengmeng Zhang, and Fujun Liu collected the information and did some experiments.

Qingyun Zeng and Qiang Wang designed the project and wrote the manuscript.

Compliance with Ethical Standards

Conflict of Interest The authors declare that they have no conflicts of interest.

References

- Biswas SK (2015) Metabolic reprogramming of immune cells in cancer progression. *Immunity* 43:435–449
- Braumann C, Koplin G, Geier C, Hohn P, Pohlenz J, Dubiel W, Rogalla S (2017) Dose-dependent role of novel agents emodin and BTB14431 in colonic cancer treatment in rats. *Acta Chir Belg* 117:376–384
- Chen WQ, Zuo TT, Zheng RS, Zeng HM, Zhang SW, He J (2017) Lung cancer incidence and mortality in China in 2013. *Zhonghua zhong liu za zhi [Chinese journal of oncology]* 39:795–800
- Chen Q, Li KT, Tian S, Yu TH, Yu LH, Lin HD, Bai DQ (2018) Photodynamic therapy mediated by aloe-emodin inhibited angiogenesis and cell metastasis through activating MAPK signaling pathway on HUVECs. *Technol Cancer Res Treat* 17: 1533033818785512
- Chen X, Mangala LS, Mooberry L, Bayraktar E, Dasari SK, Ma S, Ivan C, Court KA, Rodriguez-Aguayo C, Bayraktar R, Raut S, Sabnis N, Kong X, Yang X, Lopez-Berestein G, Lacko AG, Sood AK (2019) Identifying and targeting angiogenesis-related microRNAs in ovarian cancer. *Oncogene*
- Cheng TM, Murad YM, Chang CC, Yang MC, Baral TN, Cowan A, Tseng SH, Wong A, Mackenzie R, Shieh DB, Zhang J (2014) Single domain antibody against carcinoembryonic antigen-related cell adhesion molecule 6 (CEACAM6) inhibits proliferation, migration, invasion and angiogenesis of pancreatic cancer cells. *Eur J Cancer (Oxford, England : 1990)* 50:713–721
- Fernand VE, Losso JN, Truax RE, Villar EE, Bwambok DK, Fakayode SO, Lowry M, Warner IM (2011) Rhein inhibits angiogenesis and the viability of hormone-dependent and -independent cancer cells under normoxic or hypoxic conditions in vitro. *Chem Biol Interact* 192:220–232
- Frezza D, Gallo M, Maiello MR, D'Alessio A, Esposito C, Chicchinelli N, Normanno N, De Luca A (2017) VEGF as a potential target in lung cancer. *Expert Opin Ther Targets* 21:959–966
- He ZH, Zhou R, He MF, Lau CB, Yue GG, Ge W, But PP (2011) Anti-angiogenic effect and mechanism of rhein from *Rhizoma Rhei*. *Phytomed : Int J Phytother Phytopharmacol* 18:470–478
- Hirsch FR, Scagliotti GV, Mulshine JL, Kwon R, Curran WJ Jr, Wu YL, Paz-Ares L (2017) Lung cancer: current therapies and new targeted treatments. *Lancet (London, England)* 389:299–311
- Hong QY, Wu GM, Qian GS, Hu CP, Zhou JY, Chen LA, Li WM, Li SY, Wang K, Wang Q, Zhang XJ, Li J, Gong X, Bai CX (2015) Prevention and management of lung cancer in China. *Cancer* 121(Suppl 17):3080–3088
- Hsiao YH, Hsieh MJ, Yang SF, Chen SP, Tsai WC, Chen PN (2019) Phloretin suppresses metastasis by targeting protease and inhibits cancer stemness and angiogenesis in human cervical cancer cells. *Phytomed : Int J Phytother Phytopharmacol* 62:152964
- Hu L, Cui R, Liu H, Wang F (2017) Emodin and rhein decrease levels of hypoxia-inducible factor-1 α in human pancreatic cancer cells and attenuate cancer cachexia in athymic mice carrying these cells. *Oncotarget* 8:88008–88020
- Huang JY, Jian ZH, Nfor ON, Ku WY, Ko PC, Lung CC, Ho CC, Pan HH, Huang CY, Liang YC, Liaw YP (2015) The effects of pulmonary diseases on histologic types of lung cancer in both sexes: a population-based study in Taiwan. *BMC Cancer* 15:834
- Irwin DC, McCord JM, Nozik-Grayck E, Beckly G, Foreman B, Sullivan T, White MT, Crossno JJ, Bailey D, Flores SC, Majka S, Klemm D, van Patot MC (2009) A potential role for reactive oxygen species and the HIF-1 α -VEGF pathway in hypoxia-induced pulmonary vascular leak. *Free Radic Biol Med* 47:55–61
- Izgi K, Canatan H, Iskender B (2017) Current status in cancer cell reprogramming and its clinical implications. *J Cancer Res Clin Oncol* 143:371–383
- Jurikova M, Danihel L, Polak S, Varga I (2016) Ki67, PCNA, and MCM proteins: markers of proliferation in the diagnosis of breast cancer. *Acta Histochem* 118:544–552
- Kang DY, Sp N, Kim DH, Joung YH, Lee HG, Park YM, Yang YM (2018) Salidroside inhibits migration, invasion and angiogenesis of MDAMB 231 TNBC cells by regulating EGFR/Jak2/STAT3 signaling via MMP2. *Int J Oncol* 53:877–885
- Kebsa W, Lahouel M, Rouibah H, Zihlif M, Ahram M, Abu-Irmaileh B, Mustafa E, Al-Ameer HJ, Al Shhab M (2018) Reversing multidrug resistance in chemo-resistant human lung adenocarcinoma (A549/DOX) cells by Algerian propolis through direct inhibiting the P-gp Efflux-pump, G0/G1 cell cycle arrest and apoptosis induction. *Anti Cancer Agents Med Chem* 18:1330–1337
- Kim ES (2016) Chemotherapy resistance in lung cancer. *Adv Exp Med Biol* 893:189–209
- Kitajima N, Numaga-Tomita T, Watanabe M, Kuroda T, Nishimura A, Miyano K, Yasuda S, Kuwahara K, Sato Y, Ide T, Birnbaumer L, Sumimoto H, Mori Y, Nishida M (2016) TRPC3 positively regulates reactive oxygen species driving maladaptive cardiac remodeling. *Sci Rep* 6:37001
- Koyuncu I, Gonel A, Kocyigit A, Temiz E, Durgun M, Supuran CT (2018) Selective inhibition of carbonic anhydrase-IX by sulphonamide derivatives induces pH and reactive oxygen species-mediated apoptosis in cervical cancer HeLa cells. *J Enzyme Inhibition Med Chem* 33:1137–1149
- Kuusk T, Albiges L, Escudier B, Grivas N, Haanen J, Powles T, Bex A (2017) Antiangiogenic therapy combined with immune checkpoint blockade in renal cancer. *Angiogenesis* 20:205–215
- Lee MS, Cha EY, Sul JY, Song IS, Kim JY (2011) Chrysophanic acid blocks proliferation of colon cancer cells by inhibiting EGFR/mTOR pathway. *Phytother Res: PTR* 25:833–837
- Li X, Chen C, Dai Y, Huang C, Han Q, Jing L, Ma Y, Xu Y, Liu Y, Zhao L, Wang J, Sun X, Yao X (2019a) Cinobufagin suppresses colorectal cancer angiogenesis by disrupting the endothelial mammalian target of rapamycin/hypoxia-inducible factor 1 α axis. *Cancer Sci* 110: 1724–1734
- Li HM, Miao J, Zhu M, Gao M, Dai Y, Huo Q, Ma T, Wu CZ (2019b) Bishonokiol A inhibits breast cancer cell invasion and migration by suppressing hypoxia inducible factor-1 α . *J Bioenerg Biomembr* 51:239–248
- Liam CK, Andarini S, Lee P, Ho JC, Chau NQ, Tscheikuna J (2015) Lung cancer staging now and in the future. *Respirology (Carlton, Vic)* 20: 526–534
- Lim W, Yang C, Bazer FW, Song G (2017) Chrysophanol induces apoptosis of choriocarcinoma through regulation of ROS and the AKT and ERK1/2 pathways. *J Cell Physiol* 232:331–339
- Lim W, An Y, Yang C, Bazer FW, Song G (2018) Chrysophanol induces cell death and inhibits invasiveness via mitochondrial calcium overload in ovarian cancer cells. *J Cell Biochem* 119:10216–10227
- Liu Y, Bunston C, Hodson N, Resaul J, Sun PH, Cai S, Chen G, Gu Y, Satherley LK, Bosanquet DC, Al-Sarireh B, Tian X, Hao C, Jiang WG, Ye L (2017) Psoriasin promotes invasion, aggregation and survival of pancreatic cancer cells; association with disease progression. *Int J Oncol* 50:1491–1500
- Mao G, Liu Y, Fang X, Liu Y, Fang L, Lin L, Liu X, Wang N (2015) Tumor-derived microRNA-494 promotes angiogenesis in non-small cell lung cancer. *Angiogenesis* 18:373–382
- Mao Z, Xu B, He L, Zhang G (2019) PVT1 promotes angiogenesis by regulating miR-29c/vascular endothelial growth factor (VEGF)

- signaling pathway in non-small-cell lung cancer (NSCLC). *Med Sci Monitor : Int Med J Exp Clin Res* 25:5418–5425
- Merchant N, Nagaraju GP, Rajitha B, Lammata S, Jella KK, Buchwald ZS, Lakka SS, Ali AN (2017) Matrix metalloproteinases: their functional role in lung cancer. *Carcinogenesis* 38:766–780
- Naylor EC, Desani JK, Chung PK (2016) Targeted therapy and immunotherapy for lung cancer. *Surg Oncol Clin N Am* 25:601–609
- Netea-Maier RT, Smit JWA, Netea MG (2018) Metabolic changes in tumor cells and tumor-associated macrophages: a mutual relationship. *Cancer Lett* 413:102–109
- Njah K, Chakraborty S, Qiu B, Arumugam S, Raju A, Pobbati AV, Lakshmanan M, Tergaonkar V, Thibault G, Wang X, Hong W (2019) A role of agrin in maintaining the stability of vascular endothelial growth factor receptor-2 during tumor angiogenesis. *Cell reports* 28: 949–965.e947
- Ramjiawan RR, Griffioen AW, Duda DG (2017) Anti-angiogenesis for cancer revisited: is there a role for combinations with immunotherapy? *Angiogenesis* 20:185–204
- Ren L, Li Z, Dai C, Zhao D, Wang Y, Ma C, Liu C (2018) Chrysophanol inhibits proliferation and induces apoptosis through NF-kappaB/cyclin D1 and NF-kappaB/Bcl-2 signaling cascade in breast cancer cell lines. *Mol Med Rep* 17:4376–4382
- Shay G, Lynch CC, Fingleton B (2015) Moving targets: emerging roles for MMPs in cancer progression and metastasis. *Matrix Biol : J Int Soc Matrix Biol* 44–46:200–206
- Shi GH, Zhou L (2018) Emodin suppresses angiogenesis and metastasis in anaplastic thyroid cancer by affecting TRAF6-mediated pathways in vivo and in vitro. *Mol Med Rep* 18:5191–5197
- Song G, Zhang Y, Yu S, Lv W, Guan Z, Sun M, Wang J (2019) Chrysophanol attenuates airway inflammation and remodeling through nuclear factor-kappa B signaling pathway in asthma. *Phytotherapy research : PTR*
- Torre LA, Siegel RL, Jemal A (2016) Lung cancer statistics. *Adv Exp Med Biol* 893:1–19
- Viallard C, Larrivee B (2017) Tumor angiogenesis and vascular normalization: alternative therapeutic targets. *Angiogenesis* 20:409–426
- Wu J, Ke X, Wang W, Zhang H, Ma N, Fu W, Zhao M, Gao X, Hao X, Zhang Z (2016) Aloe-emodin suppresses hypoxia-induced retinal angiogenesis via inhibition of HIF-1alpha/VEGF pathway. *Int J Biol Sci* 12:1363–1371
- Zanin R, Pegoraro S, Ros G, Ciani Y, Piazza S, Bossi F, Bulla R, Zennaro C, Tonon F, Lazarevic D, Stupka E, Sgarra R, Manfioletti G (2019) HMGA1 promotes breast cancer angiogenesis supporting the stability, nuclear localization and transcriptional activity of FOXM1. *J Exp Clin Cancer Res* 38:313
- Zou X, Jia M, Wang X, Zhi X (2017) Changing epidemic of lung cancer & tobacco and situation of tobacco control in China. *Zhongguo fei ai za zhi = Chinese Journal of Lung Cancer* 20:505–510

Publisher's note Springer Nature remains neutral with regard to jurisdictional claims in published maps and institutional affiliations.